AAS 09-226

INVARIANT MANIFOLDS, DISCRETE MECHANICS, AND TRAJECTORY DESIGN FOR A MISSION TO TITAN

Evan S. Gawlik*, Jerrold E. Marsden†, Stefano Campagnola‡, Ashley Moore§

With an environment comparable to that of primordial Earth, a surface strewn with liquid hydrocarbon lakes, and an atmosphere denser than that of any other moon in the solar system, Saturn's largest moon Titan is a treasure trove of potential scientific discovery and is the target of a proposed NASA mission scheduled for launch in roughly one decade. A chief consideration associated with the design of any such mission is the constraint imposed by fuel limitations that accompany the spacecraft's journey between celestial bodies. In this study, we explore the use of patched three-body models in conjunction with a discrete mechanical optimization algorithm for the design of a fuel-efficient Saturnian moon tour focusing on Titan. In contrast to the use of traditional models for trajectory design such as the patched conic approximation, we exploit subtleties of the three-body problem, a classic problem from celestial mechanics that asks for the motion of three masses in space under mutual gravitational interaction, in order to slash fuel costs. In the process, we demonstrate the aptitude of the DMOC (Discrete Mechanics and Optimal Control) optimization algorithm in handling celestial mechanical trajectory optimization problems.

INTRODUCTION

Saturn's moon Titan is a treasure trove of potential scientific discovery. With an environment comparable to that of primordial Earth and an atmosphere denser than that of any other moon in the solar system,[1] Titan is so shrouded in intrigue that it has even been named a potential sustainer of extraterrestrial life.[2] The Cassini-Huygens mission's recent discovery of hydrocarbon lakes on the surface of Titan[3] has so inspired the National Aeronautics and Space Administration (NASA) that it plans to deploy a mission to Titan again in roughly one decade.

A chief consideration associated with the design of any such mission is the constraint imposed by fuel limitations that accompany the spacecraft's journey between celestial bodies. By minimizing fuel costs associated with orbital maneuvers, a well-designed trajectory can simultaneously decrease mission expenses, increase the carrying capacity of the spacecraft, and broaden the realm of visitable sites en route. This is especially important in light of the fact that NASA has expressed interest in expanding the Titan mission to include a flyby of Saturn's geologically active moon Enceladus, as well as other moons of Saturn if such a route proves feasible.

For a complex mission like a Saturnian moon tour, multi-body dynamics play a prominent role. Exploiting the natural dynamics of the three-body problem, a classic problem from celestial me-

*Control and Dynamical Systems, California Institute of Technology, MC 107-81, Pasadena, California 91125, USA. Email: egawlik@caltech.edu

†Control and Dynamical Systems, California Institute of Technology, MC 107-81, Pasadena, California 91125, USA. Email: jmarsden@caltech.edu

‡Aerospace and Mechanical Engineering, University of Southern California, 854 Downey Way, Los Angeles, California 90089-1191, USA. Email: scampagn@usc.edu

§Control and Dynamical Systems, California Institute of Technology, MC 107-81, Pasadena, California 91125, USA. Email: moore.ashley@gmail.com

chanics that asks for the motion of three masses in space under mutual gravitational interaction, has been shown to greatly improve fuel efficiency for missions of this type.[4] Traditional models used to design mission trajectories involve the so-named patched conic approximation, which divides the problem into a mosaic of two-body problems: when the spacecraft is near a mass like a planet, only that planet's influence on the craft is considered; when the spacecraft exits the planet's "sphere of influence," it enters that of another body and only the new body's gravitational effects are considered.[5] If one instead treats the problem as a patchwork of three-body problems (the Saturn-Titan-spacecraft and the Saturn-Enceladus-spacecraft systems, for example), new classes of fuel-efficient trajectories emerge. NASA's Genesis Discovery mission, for instance, exploited subtleties in the dynamics of the Sun-Earth-spacecraft system to traverse a route whose intricacies simpler models like the patched conic approximation fail to describe adequately.[6] The key feature of the three-body problem that permits such dramatic improvement to space mission design is the presence of invariant manifolds—sets of points in the system's phase space that tend toward a given limiting set as time tends to plus or minus infinity—of certain periodic solutions to the three-body problem equations of motion. As Koon and co-authors[7] demonstrate, a globalization of the stable and unstable manifolds of periodic orbits about the L_1 and L_2 Lagrange points (unstable equilibrium points in the the circular restricted three-body problem) reveals a web of tubes through phase space that form separatrices between its dynamically different regions. This labyrinth of cylindrical tubes, dubbed an "interplanetary transport network,"[5] can be exploited to design trajectories that use extremely little fuel to navigate complex routes.

In this study, we explore the use of patched three-body models in conjunction with a discrete mechanical optimization algorithm for the design of a fuel-efficient Saturnian moon tour focusing on Titan. To achieve this goal, we begin by giving an introduction to tube dynamics in the circular restricted three-body problem, followed by a description of the DMOC (Discrete Mechanics and Optimal Control) optimization algorithm. We then demonstrate the manner in which these tools can be applied to a well-studied trajectory design problem, namely the problem of constructing a low-fuel trajectory from the Earth to the Moon. Finally, we couple the theory of invariant manifolds with the use of resonant gravity assists in order to design a fuel-efficient tour of the Saturnian moon system.

METHODS

This section provides background material on the tools to be used in the subsequent section for space mission trajectory design: the circular restricted three-body problem (CR3BP), invariant manifolds in the CR3BP, and the DMOC (Discrete Mechanics and Optimal Control) optimization algorithm.

The Circular Restricted Three-Body Problem (CR3BP)

The circular restricted three-body problem (CR3BP) considers the motion of a test mass $m_3 = 0$ in the presence of the gravitational field of two primary masses $m_1 = 1 - \mu$ and $m_2 = \mu$ in circular orbit about their center of mass. Throughout the paper, all motion is assumed to take place within the m_1-m_2 orbital plane. Without loss of generality, all units are normalized and positions are defined relative to a rotating coordinate frame whose x-axis coincides with the line joining m_1 and m_2 and whose origin coincides with the center of mass of m_1 and m_2, as shown in Fig. 1. The equations of

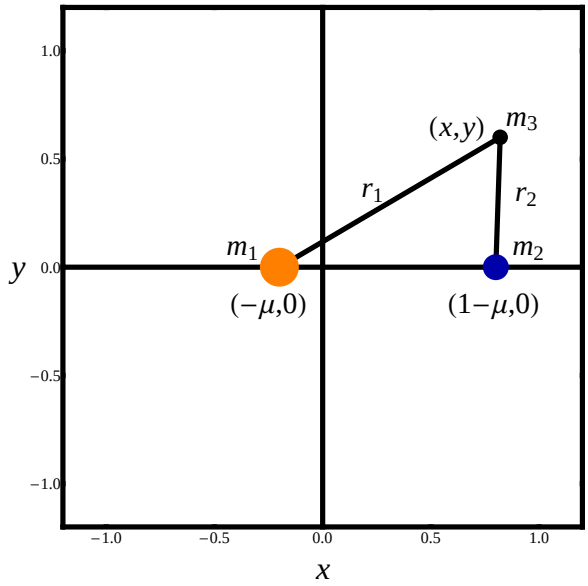

Figure 1 Rotating coordinate system in the circular restricted three-body problem. All units are nondimensionalized. The coordinate frame rotates counterclockwise with unit angular frequency so that the primary masses m_1 and m_2 remain fixed at the positions $(-\mu, 0)$ and $(1-\mu, 0)$, respectively.

motion for the test particle are then

$$\ddot{x} - 2\dot{y} = \frac{\partial \Omega}{\partial x} \tag{1}$$

$$\ddot{y} + 2\dot{x} = \frac{\partial \Omega}{\partial y}, \tag{2}$$

where

$$\Omega(x,y) = \frac{x^2+y^2}{2} + \frac{1-\mu}{\sqrt{(x+\mu)^2+y^2}} + \frac{\mu}{\sqrt{(x-1+\mu)^2+y^2}} + \frac{1}{2}\mu(1-\mu) \tag{3}$$

and (x, y) denotes the position of m_3 in the rotating frame.[8]

There are five equilibrium points (Lagrange points) L_i, $i = 1, 2, 3, 4, 5$, in the CR3BP,[8] corresponding to critical points of the effective potential Ω. Three of these points (L_1, L_2, and L_3) are collinear with the masses m_1 and m_2, while the remaining two (L_4 and L_5) lie at the vertices of the pair of equilateral triangles whose bases coincide with the line segment joining m_1 and m_2 (see Fig. 2(b)). Let L_i^x and L_i^y denote the x and y coordinates, respectively, of i^{th} Lagrange point.

It is straightforward to check through differentiation that

$$E(x, y, \dot{x}, \dot{y}) = \frac{1}{2}(\dot{x}^2 + \dot{y}^2) - \Omega(x, y) \tag{4}$$

is a constant of motion for the CR3BP. We shall refer to this constant as the energy of the system. Throughout this report, $E(L_i)$ shall denote the energy of the i^{th} Lagrange point, i.e. $E(L_i) =$

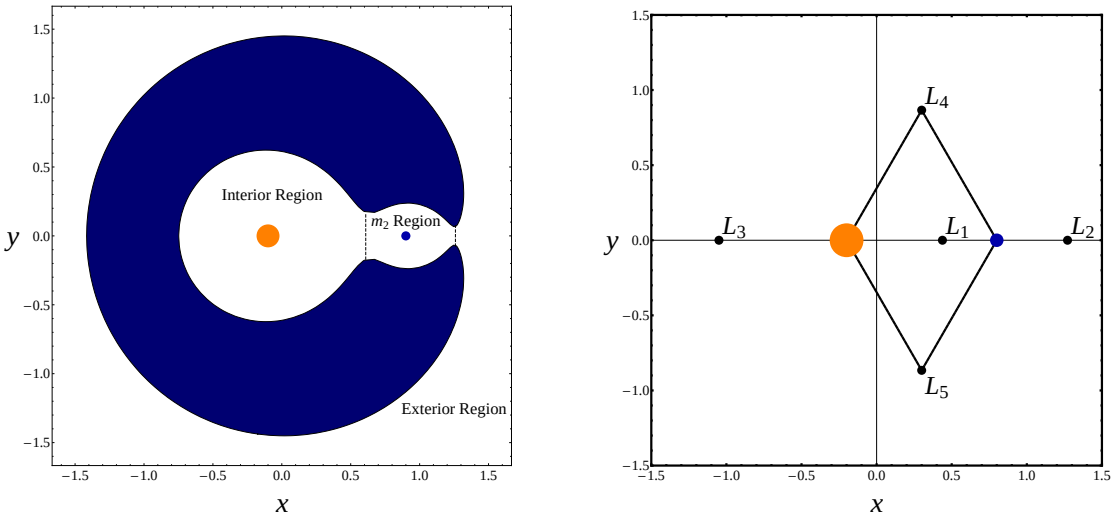

(a) (b)

Figure 2 (a) Regions of allowed motion (white areas) in the circular restricted three-body problem with $\mu = 0.1$, $E = -1.775$. (b) Equilibrium points L_i, $i = 1, 2, 3, 4, 5$, in the circular restricted three-body problem with $\mu = 0.1$.

$E(L_i^x, L_i^y, 0, 0)$. Since E is constant in the CR3BP and $(\dot{x}^2 + \dot{y}^2)$ is a nonnegative quantity, it immediatelly follows that m_3 is restricted to regions of the (x, y) plane where

$$-\Omega(x, y) \leq E. \tag{5}$$

Moreover, a given particle in the CR3BP is constrained to a three-dimensional energy surface $\mathcal{M} = \{(x, y, \dot{x}, \dot{y}) \mid E(x, y, \dot{x}, \dot{y}) = const.\}$ defined by its initial energy.

Invariant Manifolds

The presence of forbidden regions in the CR3BP permits the definition of three subsets of the (x, y) plane when $E(L_2) < E < E(L_3)$: the interior, m_2, and exterior regions, bounded approximately by the lines $x = L_1^x$, $x = L_2^x$, and the boundary of the forbidden regions (see Fig. 2(a)). A natural question to pose now is the following: What regulates the transport of particles between the interior, m_2, and exterior regions in the CR3BP?

Koon and co-authors[7] provide the answer to this question through analysis of the invariant manifolds of periodic orbits in the CR3BP. By linearizing the equations of motion at the collinear Lagrange points, the authors show that these equilibrium points have the stability type $saddle \times center$. Consequently, there exists a family of periodic orbits (called Lyapunov orbits) about L_i for each $i \in \{1, 2, 3\}$, whose stable and unstable manifolds form cylindrical tubes ($S^1 \times \mathbb{R}$). Within a surface of constant energy, these tubes (as shown in Fig. 3) form codimension-1 separatrices between orbits with different fates: transit orbits, which exit one region and enter an adjacent region; and non-transit orbits, which remain entrapped in the region in which they began. More precisely, a particle with energy E that is currently in a given region R_A will enter an adjacent region R_B under the forward (respectively, backward) time flow if and only if that particle is inside the stable (respectively, unstable) manifold tube emanating from the unique periodic orbit of energy E associated with the Lagrange point that lies on the shared boundary of regions R_A and R_B.

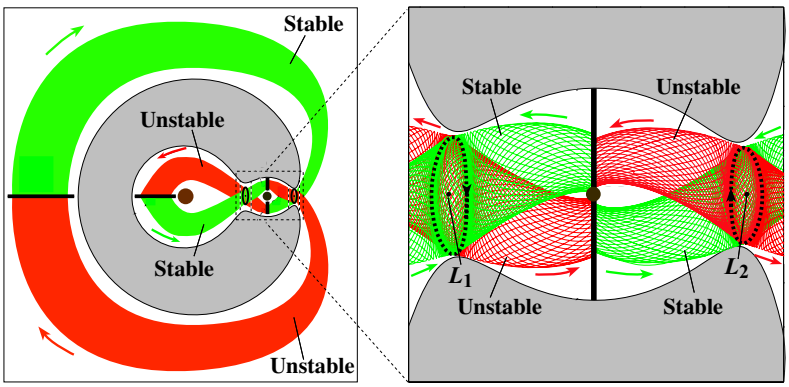

Figure 3 Projection of the stable (green) and unstable (red) manifold tubes in the CR3BP onto position space. Image borrowed from Gomez *et al.*.[9]

Computational methods for determining the CR3BP invariant manifolds are well-developed.[10,11] To sumarize the procedure, one first constructs a periodic orbit with a specified energy using differential correction. The evolution of the periodic orbit's state transition matrix is computed over one period, and local approximations of the stable and unstable manifolds of the periodic orbit are obtained from the eigenvectors of that state transition matrix. A set of tracers in the directions of the stable and unstable eigenspaces can then be advected under the full nonlinear equations of motion to generate the invariant manifolds. The process can be curtailed by exploiting a symmetry in the CR3BP equations of motion: the mapping $(x, y, \dot{x}, \dot{y}, t) \mapsto (x, -y, -\dot{x}, \dot{y}, -t)$ is a symmetry of equations (1-2); as a result, the unstable manifold of a given Lyapunov orbit can be found by negating the y and $\dot{x}$ coordinates of every point on the corresponding stable manifold.

Discrete Mechanics and Optimal Control (DMOC)

DMOC (short for Discrete Mechanics and Optimal Control) is an algorithm designed for the solution of optimal control problems for which the underlying dynamical system is mechanical in nature.[12] As such, DMOC is well-suited for the design of space mission trajectories, where one seeks to utilize control forces to target desirable destinations in a multi-body dynamics problem, using as little fuel as possible and meeting various time constraints. Often the aim is to minimize a trajectory's total ΔV, the sum of the spacecraft's instantaneous velocity changes spawning from thrusts applied over the course of its flight. In order to execute such a minimization, one must have a means of numerically integrating the system's equations of motion. For mechanical systems like the three-body problem, numerical integration algorithms which respect the structure of the mechanical system at hand by accurately capturing the evolution of quantities like energy and momentum and respecting the symplectic nature of the system's flow are highly desirable.[13] For this reason, the DMOC algorithm relies on the use of a class of numerical integrators called variational integrators.

Variational integrators may be derived by viewing mechanical systems from the standpoint of variational mechanics. Particularly, a fundamental principle from classical mechanics called *Hamilton's principle of critical action*[14] states that a mechanical system whose configuration is described by a generalized coordinate vector $q(t)$ will evolve such that the so-called action integral

$$\int_0^T L(q(t), \dot{q}(t))\, \mathrm{d}t \tag{6}$$

is extremized subject to fixed endpoints $q(0) = q_0$ and $q(T) = q_f$, where $L(q(t), \dot{q}(t))$ is the system's kinetic energy minus potential energy at time t. Treating the curve $q(t)$ which extremizes (6) as a member $q^0(t)$ of a one-parameter family of curves $\{q^\varepsilon(t) \mid \varepsilon \in (-\varepsilon_0, \varepsilon_0) \subset \mathbb{R}\}$ satisfying $q^\varepsilon(0) = q_0$ and $q^\varepsilon(T) = q_f$ for all ε and abbreviating $\frac{\mathrm{d}}{\mathrm{d}\varepsilon}\big|_{\varepsilon=0}$ as δ, Hamilton's principle may be written succinctly as

$$\delta \int_0^T L(q(t), \dot{q}(t))\,\mathrm{d}t = 0 \tag{7}$$

for all variations $\delta q(t)$ satisfying $\delta q(0) = \delta q(T) = 0$. Calculus of variations then shows that (7) holds only if $q(t)$ satisfies the Euler-Lagrange equations:

$$\frac{\partial L}{\partial q} - \frac{\mathrm{d}}{\mathrm{d}t}\frac{\partial L}{\partial \dot{q}} = 0. \tag{8}$$

As an example, consider a particle moving in $\mathbb{R}^3$ in the presence of a potential $V(q)$, where q is the usual cartesian position vector (x, y, z). Then $L = \frac{1}{2}\dot{q}^T M \dot{q} - V(q)$ and equation (8) reduces to Newton's second law, force equals mass times acceleration:

$$M\ddot{q} = -\nabla V(q). \tag{9}$$

To derive a variational integrator, one discretizes the action integral (6) and uses a discrete version of the Euler-Lagrange equations (8) to define a map $(q_{k-1}, q_k) \mapsto (q_k, q_{k+1})$, where $q_k \approx q(kh)$ and h is a time step. This map is then applied recursively to a set of initial conditions (q_0, q_1) to produce a discrete curve of points $\{q_k\}_{k=0}^{T/h}$ that approximates $q(t)$ over the time interval $[0, T]$. Different variational integrators, possibly with differing orders of accuracy, can be constructed using different quadrature methods for the discretization of the action integral (6).[15]

Three distinguishing features of constant time-stepping variational integrators applied to conservative mechanical systems are exact momentum conservation, symplecticity (for systems with one degree of freedom, this property can be realized as preservation of area in phase space under the discrete Lagrangian map $(q_{k-1}, q_k) \mapsto (q_k, q_{k+1})$), and accurate energy behavior.[16]

We are interested in designing trajectories which utilize control forces to target desirable destinations. For instance, a mission through the Saturnian moon system might require thrust to transfer from one elliptical orbit about Saturn to another. To incorporate such forcing, we invoke a generalization of Hamilton's principle of critical action called the *Lagrange-d'Alembert principle*,[17] which says that in the presence of a non-conservative force $f(t)$, the evolution of a mechanical system is a curve $q(t)$ satisfying

$$\delta \int_0^T L(q(t), \dot{q}(t))\,\mathrm{d}t + \int_0^T f(t) \cdot \delta q(t)\,\mathrm{d}t = 0 \tag{10}$$

for all variations $\delta q(t)$ with $\delta q(0) = \delta q(T) = 0$.

To derive a mechanical integrator based upon this forced principle of critical action, we approximate the curve $q(t)$ with a discrete sequence of points $\{q_k\}_{k=0}^N$ where $q_k \approx q(kh)$ and h is a time step. We then seek solutions to

$$\delta \sum_{k=0}^{N-1} L_d(q_k, q_{k+1}, h) + \sum_{k=0}^{N-1} (f_k^- \cdot \delta q_k + f_k^+ \cdot \delta q_{k+1}) = 0, \tag{11}$$

where the action integral (6) is approximated over each subinterval $[kh, (k+1)h]$ with a discrete Lagrangian L_d satisfying

$$L_d(q_k, q_{k+1}, h) \approx \int_{kh}^{(k+1)h} L(q(t), \dot{q}(t))\,\mathrm{d}t, \tag{12}$$

and the second term of (10) is approximated with discrete forces f_k^- and f_k^+ satisfying

$$f_k^- \cdot \delta q_k + f_k^+ \cdot \delta q_{k+1} \approx \int_{kh}^{(k+1)h} f(t) \cdot \delta q(t)\,\mathrm{d}t. \tag{13}$$

In analogy with the continuous case, it can be shown that (11) is satisfied only if the sequence $\{q_k\}_{k=0}^N$ satisfies the forced discrete Euler-Lagrange equations

$$D_2 L_d(q_{k-1}, q_k, h) + D_1 L_d(q_k, q_{k+1}, h) + f_{k-1}^+ + f_k^- = 0 \tag{14}$$

for each $0 < k < N$, where $D_i L_d$ denotes the derivative of L_d with respect to its i^{th} argument.

Typically, we seek controlled trajectories which not only satisfy Newton's laws and reach desired destinations, but also minimize fuel costs, time of flight, and the like. We can encapsulate these aims by defining a cost function $J(q, f)$ which we seek to minimize. For instance, to minimize a space mission trajectory's ΔV, we set $J(q, f) = \int_0^T ||f||\,\mathrm{d}t$, approximated via numerical quadrature of definite integrals. The DMOC optimization problem can then be posed as follows: Given an initial guess trajectory $\{q_k\}_{k=0}^N$ and an initial guess control trajectory $\{f_k\}_{k=0}^{N-1}$, vary $\{q_k\}_{k=0}^N$ and $\{f_k\}_{k=0}^{N-1}$ in order to minimize the cost functional $J(q, f)$ subject to the constraint equations (14). This is an equality constrained nonlinear optimization problem, a standard problem in the field of nonlinear programming whose solution may be computed with any of a number of numerical algorithms, such as a sequential quadratic programming (SQP) routine.[18,19]

RESULTS

In this section, we demonstrate the manner in which invariant manifold theory from three-body problem, when coupled with the use of the DMOC optimal control algorithm, can be exploited to tackle a well-studied trajectory design problem often reffered to in the literature as the "Shoot the Moon" problem: the problem of constructing a low-fuel trajectory from the Earth to the Moon. We then shift our focus to Titan mission trajectory design problem, invoking a technique involving *resonant gravity assists* in order to target CR3BP invariant manifolds in the Saturn-Titan-spacecraft system and design a fuel-efficient trajectory through the Saturnian moon system.

Shoot the Moon

Consider the following problem: design a trajectory, requiring as little fuel as possible, from the Earth to the Moon. This so-called "Shoot the Moon" problem is of obvious practical importance and has been studied in detail by Koon and co-authors[20] with the aid of invariant manifolds in the circular restricted three-body problem. For the purposes of this report (and to facilitate comparison with previous results reported by Koon and co-authors,[20]) we are concerned primarily with mid-course ΔV requirements: the fuel costs of the portion of the trajectory following departure from a low-altitude Earth parking orbit.

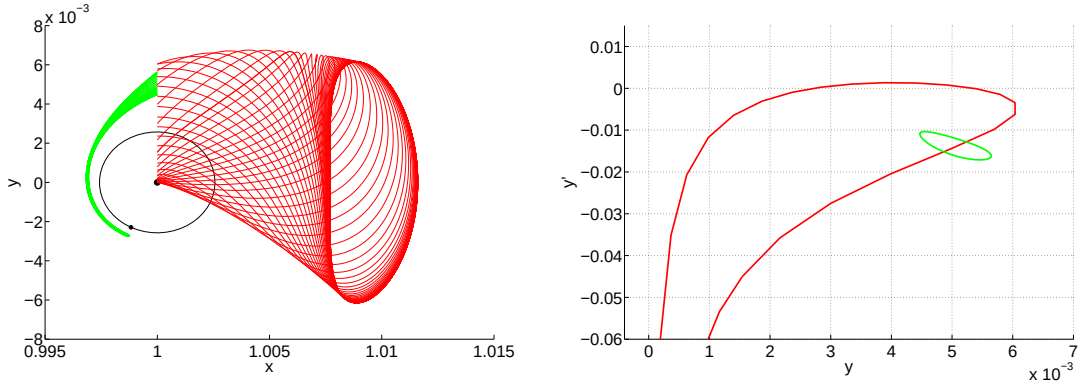

(a) (b)

Figure 4 (a) Unstable manifold (red) of an L_2 periodic orbit in the Sun-Earth-spacecraft three-body sytem, superposed with the stable manifold (green) of an L_2 periodic orbit in the Earth-Moon-spacecraft system. Coordinates are given with respect to a barycentric frame which rotates at a rate such that the Sun and Earth remain fixed on the x-axis. Units are scaled such that the Sun-Earth distance and the angular velocity of the rotating frame are both equal to unity. The central black disc denotes the Earth, while the thin black circle traces the Moon's orbit. (b) Intersection of the invariant manifold tubes depicted in (a) with the plane $x = 1 - \mu_E$, where $\mu_E = m_{Earth}/(m_{Sun} + m_{Earth})$.

To give the reader a sense of the fuel costs associated with mid-course maneuvers, it is helpful to consider the fuel requirements of a Hohmann transfer trajectory from the Earth to the Moon. A Hohmann transfer is a classic patched-conic manuever by which a spacecraft begins an initial circular orbit of radius r_1 about a given body and transfers to a final circular orbit of radius r_2 about the body by traversing a semiellipse with periapsis distance r_1 and apoapsis distance r_2. An Earth-to-Moon trajectory which utilizes a Hohmann transfer to transit from a circular 185-km altitude parking orbit about Earth to a larger circular orbit about Earth with radius matching that of the Moon's orbital radius requires roughly 3960 m/s of fuel.[21]

These fuel costs can be slashed if we employ the theory of invariant manifolds in the CR3BP developed in the previous section. In particular, we treat the problem as a mosaic of the three-body problems: initially, the spacecraft departs Earth along a path that is well-approximated as a motion in the Sun-Earth-spacecraft CR3BP. At some point, which refer to as the *patch point*, lunar effects intervene and we treat the spacecraft's path as a motion in the Earth-Moon-spacecraft CR3BP. Using this patched trajectory as an initial guess, we invoke DMOC to optimize fuel costs and obtain a trajectory fully integrated in a Sun-Earth-Moon-spacecraft four-body model. For details on the four-body model used in this report, the reader is referred to the text by Koon and co-authors.[22]

Two invariant manifolds play a special role in the "Shoot the Moon" problem: the unstable manifolds of periodic orbits about the L_2 Lagrange point in the Sun-Earth-spacecraft three-body system, and the stable manifolds of periodic orbits about the L_2 Lagrange point in the Earth-Moon-spacecraft three-body system. Following the lead of Koon *et al.*,[20] we aim to design an Earth-to-Moon trajectory (see Fig. 5) which traces the following route: (1) Depart Earth along a path destined to nearly wind onto a Sun-Earth L_2 periodic orbit, (2) "bounce" off of the Sun-Earth L_2 equilibrium region along a path which hugs the unstable manifold of that Sun-Earth L_2 periodic orbit, and (3)

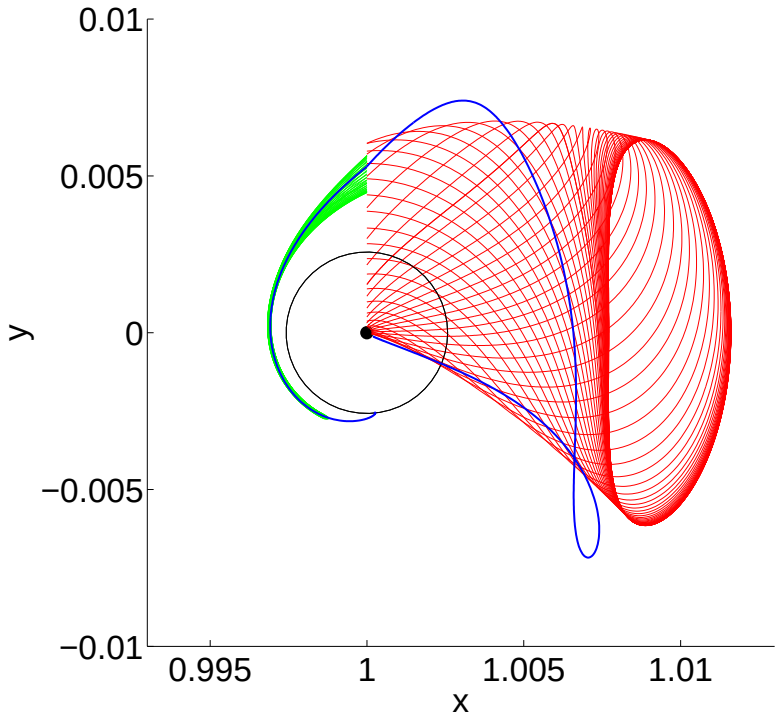

Figure 5 A patched Earth-to-Moon trajectory juxtaposed with the Sun-Earth (red) and Earth-Moon (green) invariant manifolds, in Sun-Earth rotating coordinates. The central black disc denotes the Earth, while the thin black circle traces the Moon's orbit. A ΔV of 163 m/s is required at the patch point. Additional fuel costs come from an Earth orbit departure ΔV and a lunar orbit insertion ΔV.

enter the stable manifold tube of an Earth-Moon L_2 periodic orbit and travel to the Moon. Entrance into the stable manifold tube of a lunar L_2 periodic orbit ensures that the spacecraft can achieve ballistic capture at the moon. The only ΔV requirement for this trajectory (aside from initial launch costs) is that associated with the transfer from the exterior of the Sun-Earth unstable manifold to the interior of the Earth-Moon stable manifold at the patch point.

Fig. 4 displays the unstable manifold of an L_2 periodic orbit in the Sun-Earth-spacecraft three-body system, superposed with the stable manifold of an L_2 periodic orbit in the Earth-Moon-spacecraft three-body system, all in normalized Sun-Earth rotating coordinates. Notice that in Fig. 4(b), the Sun-Earth and Earth-Moon manifolds intersect. This serendipitous intersection (due in part to a careful choice of an initial phase for the Moon) makes possible the construction of a low-ΔV trajectory from the Earth to the Moon as follows: Choose a point in the $(y, \dot{y})$ plane of Fig. 4(b) in the interior of the lobe enclosed by the Earth-Moon stable manifold but just outside the Sun-Earth unstable manifold. With the appropriate x-velocity, this point will follow the interior of the Earth-Moon stable manifold tube and achieve ballistic capture at the Moon when advected forward in time. With a slightly different x-velocity, this point can be advected backward in time toward the Sun-Earth L_2 equilibrium region. Since it is outside the Sun-Earth unstable manifold tube, it must "bounce" off the equilibrium region and hug the Sun-Earth stable manifold (not shown in the figure) back toward Earth. (The choice of a patch point lying very close to but just outside of

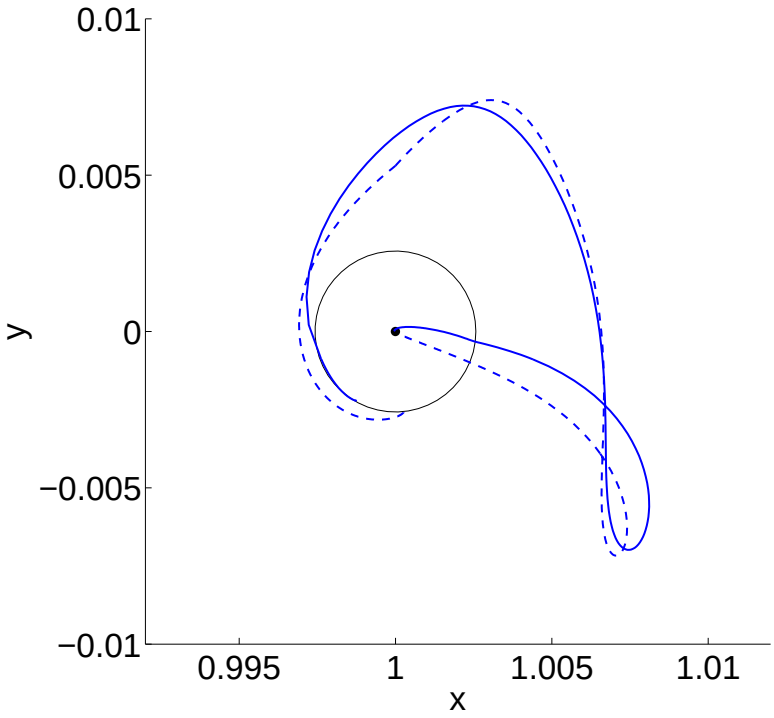

Figure 6 Locally optimal Earth-to-Moon trajectory (solid blue line) juxtaposed with the patched initial guess (dashed blue line) of Fig. 5. The central black disc denotes the Earth, while the thin black circle traces the Moon's orbit. A total ΔV cost (including Earth departure and lunar orbit insertion costs) of 3850 m/s is required for the optimal trajectory, a 110 m/s improvement over the Hohmann transfer cost of 3960 m/s.

the Sun-Earth unstable manifold ensures flexibility; a small change in inital state can lead to large changes in the final position of the spacecraft when advected backward in time from such a location, thus making the Earth-targeting portion of the design problem a feasible task. For more information, the reader is referred to the discussion of "twisting" of orbits given by Koon and co-authors.[22])

In Fig. 5, we display a patched Earth-to-Moon trajectory consisting of two pieces as described above. A ΔV of 163 m/s is required at the patch point, a value on the same order of magnitude as that given by Koon and co-authors (34 m/s) for a similar trajectory.[20] Additional ΔV's are required for departure from an Earth parking orbit and insertion into lunar orbit.

The trajectory just described is not optimal. Intuitively, a more fuel-efficient trajectory can be constructed by fine-tuning the control effort; the patched trajectory utilizes a single impulsive thrust at a more or less arbitrary position along its path. To this end, we apply DMOC to the problem of minimizing ΔV requirements, using the patched trajectory as an initial guess. To facilitate comparison with the classic Hohmann transfer approach and with the work of Perrozi & Di Salvo,[23] we impose the following boundary conditions on the spacecraft's trajectory: an initial 185-km altitude circular orbit about the Earth and a terminal 100-km altitude circular orbit about the Moon. In practice, the first constraint may be enforced by requiring the spacecraft's initial position and velocity be such that, when advected backward in time with a Runge-Kutta integrator, the spacecraft makes

ΔV (m/s)	Hohmann transfer	Multibody approach
Earth orbit departure	3150	3210
Mid-course maneuvers	0	$\tilde{0}$
Lunar orbit insertion	810	640
Total	3960	3850

Table 1 Comparison of fuel costs for a transfer from a 185-km altitude circular Earth parking orbit to a 100-km altitude circular lunar orbit. The multibody approach of Fig. 6 requires slightly more fuel for Earth orbit departure, but saves substantially during lunar orbit insertion, resulting in a net fuel savings of 110 m/s over the classic Hohmann transfer approach.

a periapsis passage with the Earth at an altitude of 185 km; the second constraint is enforced by requiring the spacecraft's final position and velocity be such that, when advected forward in time with a Runge-Kutta integrator, the spacecraft makes a periapsis passage with the Moon at an altitude of 100 km. Using the well-known formula for the velocity of a spacecraft in circular orbit about a massive body, normalized Delta-V's for the Earth orbit departure and lunar orbit insertion maneuvers may then be computed as

$$\Delta V_{Earth} = \sqrt{\dot{x}_E(t_0)^2 + \dot{y}_E(t_0)^2} - \sqrt{\frac{\mu_E}{x_E(t_0)^2 + y_E(t_0)^2}} \tag{15}$$

$$\Delta V_{Moon} = \sqrt{\dot{x}_M(t_f)^2 + \dot{y}_M(t_f)^2} - \sqrt{\frac{\mu_M}{x_M(t_f)^2 + y_M(t_f)^2}} \tag{16}$$

Here $(x_E, y_E, \dot{x}_E, \dot{y}_E)$ and $(x_M, y_M, \dot{x}_M, \dot{y}_M)$ denote normalized coordinates of the spacecraft with respect to non-rotating frames whose origins coincide with the Earth and Moon, respectively; t_0 and t_f denote the times at which the spacecraft makes its periapsis passages with respect to the Earth and Moon, respectively; and μ_E and μ_M denote the masses of the Earth and Moon in normalized units.

The optimized trajectory generated through application of the DMOC algorithm, using the patched trajectory of Fig. 5 as an initial guess, is displayed in Fig. 6. The total ΔV requirement for this trajectory (including Earth orbit departure and lunar orbit insertion costs) is 3850 m/s, in good agreement with the numbers reported by Perrozi & Di Salvo.[23] Relative to the 3960 m/s required for an Earth-to-Moon Hohmann transfer, the trajectory of Fig. 6 is considerably more fuel-efficient. The fuel savings, of course, come at a cost: while a Hohmann transfer takes just 5 days to execute, the trajectory in Fig. 6 has a flight time of roughly 6 months. Nevertheless, trajectories like that of Fig. 6 are well-suited for unmanned missions, where short flight times may safely be sacrificed for fuel savings.

Resonant Gravity Assists and the Titan Mission

The low-fuel "Shoot the Moon" trajectory of Fig. 6 was made possible by a fortuitous intersection of the invariant manifolds of the Sun-Earth-spacecraft and Earth-Moon-spacecraft three-body systems. In a general celestial system, the distances between primary bodies and their relative masses may not permit such fortunate circumstances. In particular, it has been observed numerically that

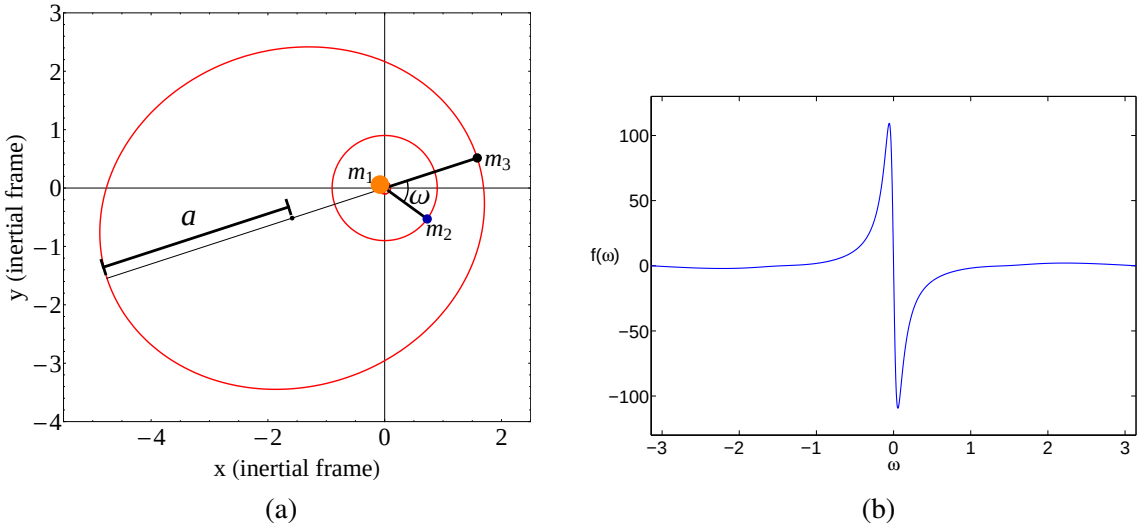

(a) (b)

Figure 7 (a) Osculating orbital elements ω and a in the CR3BP, viewed from an inertial frame. ω is the argument of periapsis of m_3's near-elliptical orbit with respect to the m_1-m_2 barycenter, and a is the instantaneous semimajor axis of m_3's orbit. In practice, a is computed as $a = -1/(2K)$, where K is the instantaneous Keplerian energy of m_3: $K = \frac{1}{2}((\dot{x}-y)^2 + (\dot{y}+x)^2) - 1/\sqrt{x^2+y^2}$. (b) Plot of the *energy kick function* $f(\omega)$ for a fixed value of the Jacobi constant C_J and Keplerian energy K. Notice that for values of ω just above zero, f takes on large negative values. Physically, this says that the Keplerian energy of a spacecraft which makes a periapsis passage just ahead of m_2 in the exterior region of the CR3BP receives a large negative kick, leading to a decrease in the semimajor axis a of the spacecraft's orbit about the m_1-m_2 barycenter.

the invariant manifolds of the Saturn-Titan-spacecraft system do not pass near the invariant manifolds of the Lyapunov orbits associated with Saturn's other moons, a situtation that can be partly attributed to the small masses of Saturn's non-Titanian moons.

To overcome this barrier, it is possible to utilize repeated gravitational assists to iteratively modify the osculating orbital elements of a spacecraft in orbit about Saturn and steer it toward sequential flybys at multiple moons. Such techniques have formerly been applied to the design of a trajectory through the Jovian moon system which requires very low amounts of fuel.[24] Dubbed a "Multi-Moon Orbiter," the trajectory begins in a Jovian orbit with semimajor axis larger than Jupiter's outermost major moon and performs resonant gravity assists with the major moons in sequence to gradually reduce the orbit's semimajor axis and visit multiple moons en route.

To facilitate the design problem, Ross and Scheeres[25] derive a map which approximates the change in orbital elements over one period of a particle in orbit in the exterior region of the circular restricted three-body problem with a small mass parameter μ. Given a particle in orbit with Jacobi constant $C_J = -2E$, instantaneous Keplerian energy $K = -1/(2a)$ (where a denotes instantaneous semimajor axis), and argument of periapsis ω with respect to the rotating frame, the map approximates the orbit's change in Keplerian energy and argument of periapsis between successive arrivals at periapsis as

$$\begin{pmatrix} \omega_{n+1} \\ K_{n+1} \end{pmatrix} = \begin{pmatrix} \omega_n - 2\pi(-2K_{n+1})^{-3/2} & \mod 2\pi \\ K_n + \mu f(\omega_n) \end{pmatrix}, \tag{17}$$

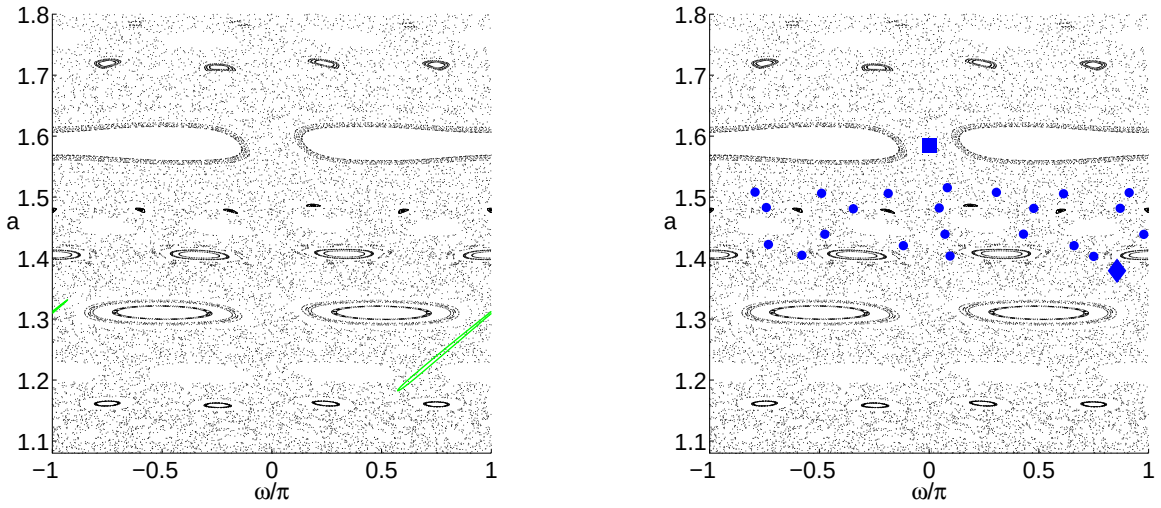

Figure 8 (a) Poincare section taken at periapsis for orbits in the exterior region of the Saturn-Titan system ($\mu = 2.366 \times 10^{-4}$), generated using the discrete Keplerian map (17). Axes are the instantaenous semimajor axis $a = -1/(2K)$ and argument of periapsis ω for the particle's orbit at the moment of periapsis. The green curve in the lower right-hand corner corresponds to the intersection of the stable manifold of an L_2 periodic orbit with the surface of section. The curve encloses a lobe of capture trajectories: sets of trajectories which, upon the next iterate of the Poincaré map, enter the Titan region of position space. (b) Example of a resonance-hopping trajectory in the Saturn-Titan system which quickly decreases its semimajor axis after several revolutions. The square and diamond denote the initial and final points, respectively, along the sequence of iterates marked in blue.

where f is the so-called *energy kick function*,[25] a function depending parametrically on C_J and K which can be computed via numerical quadrature. A plot of the kick function f, together with a diagram of the orbital elements just described, is given in Fig. 7.

A plot of successive iterates of the Keplerian map for the Saturn-Titan system is given in Fig. 8. The image was generated by seeding a region of the (ω, K) cylinder with a 10×10 grid of points with Jacobi constant $C_J = 3.014$ and plotting their locations after 250 iterates of the map (17), where the parametric dependence of f on K was eliminated by fixing a reference Keplerian energy $\bar{K} = -1/(2\bar{a})$ ($\bar{a} = 1.3$), an approximation advocated by Ross and Scheeres.[25] Included in Fig. 8(a) is a plot of the intersection of the stable manifold of an L_2 periodic orbit with the surface of section. The curve encloses a lobe of capture trajectories: sets of trajectories which, upon the next iterate of the Poincaré map, enter the Titan region of position space.

Ideally, we would like to find orbits which migrate from the upper portion of Fig. 8(a) to the lower portion and enter the green stable manifold tube. Such orbits, when plotted in position space, correspond to trajectories which start with a large semimajor axis, decrease in semimajor axis via the use of resonant gravity assists, and enter the stable manifold tube of a Saturn-Titan L_2 periodic orbit, a natural pathway leading to capture at Titan or entrance into the Saturn-Titan interior region.

To design such a trajectory, we implement an algorithm similar to that outlined by Grover and

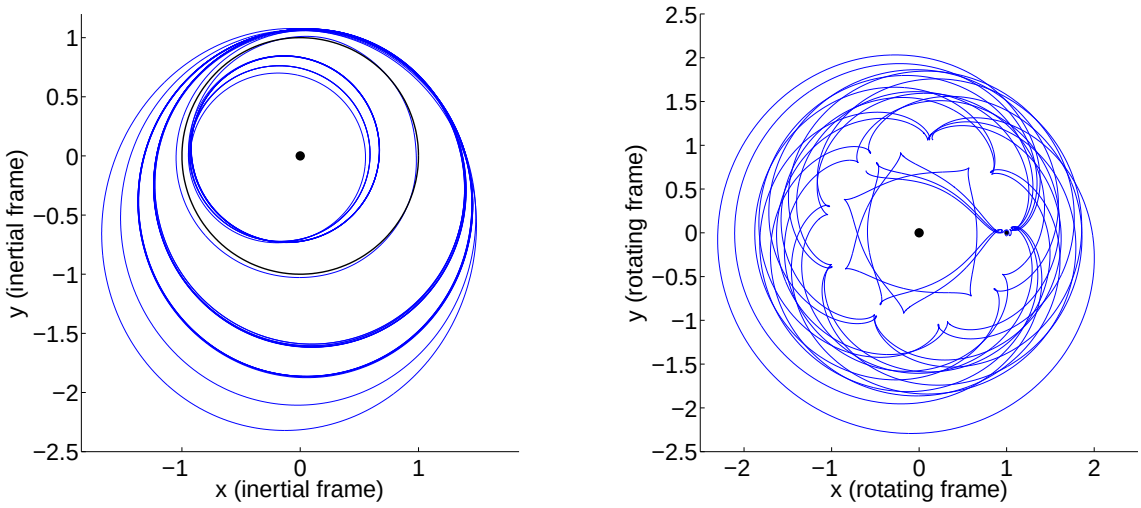

(a) (b)

Figure 9 (a) Trajectory in the Saturn-Titan CR3BP which utilizes resonant gravity assists with Titan in order to iteratively reduce the orbit's semimajor axis. Over the course of its 23-month flight, the trajectory requires a surprisingly small total ΔV: just 8 m/s. The central black disc denotes Saturn, and the thin black circle traces Titan's orbit. (b) The same trajectory, plotted in a rotating frame with Saturn and Titan fixed on the x-axis.

Ross[26] in their studies of Jovian Multi-Moon Orbiter design. Starting from an orbit with semimajor axis $a > 1$ and Jacobi constant $C_J < -2E(L_2)$ in the exterior region of the Saturn-Titan CR3BP position space, we advect the orbit forward in time until a periapsis passage is made whose argument is within a small user-defined interval containing ω_{min}, the value of the periapsis angle for which the energy kick function $f(\omega)$ takes on its most negative value. Using small impulsive velocity changes at periapsis and apoapsis passages, we refine the uncontrolled trajectory so that the final iterate has an argument of periapsis exactly equal to ω_{min}. The refinement may be carried out through the use of a root solver (to target ω_{min}) followed by an equality constrained minimization (to minimize net ΔV). Starting from the endpoint of this trajectory segment, we propogate the trajectory forward in time until a periapsis passage is again made near ω_{min}. We target ω_{min} using small ΔV's over the current trajectory segment and repeat this procedure, iteratively reducing the semimajor axis of the spacecraft's orbit each time a periapsis passage is made at ω_{min}. Once an iterate lands near the stable manifold tube of the Saturn-Titan L_2 Lyapunov orbit with energy $-1/(2C_J)$, we target the interior of the stable manifold tube using small ΔV's, thereby permitting entrance into the interior region of position space. An identical procedure may then be used in the interior region of position space to repeatedly target minima of the energy kick function and iteratively reduce the semimajor axis of the spacecraft's orbit.

Fig. 9 displays a trajectory in the Saturn-Titan-spacecraft three-body problem generated using the algorithm described above. The trajectory begins in a near-elliptical orbit about the Saturn-Titan barycenter with a semimajor axis of 1.70 Saturn-Titan distances, uses small ΔV's to take maximal advantage of repeated resonant gravity assists with Titan, and reduces the size of its orbit to one with a final semimajor axis of 0.74 Saturn-Titan distances. Over the course of its 23-month flight, the

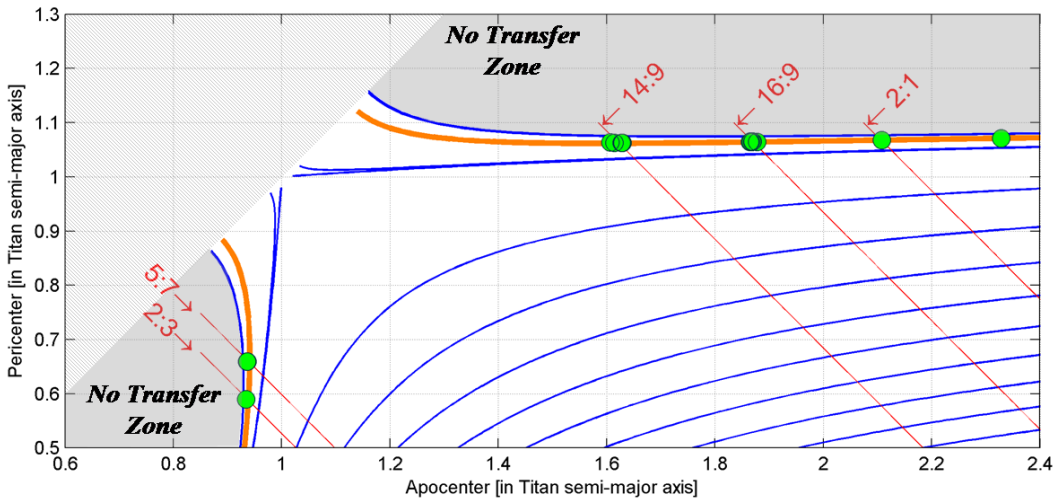

Figure 10 Graph depicting the evolution of the pericenter and apocenter of the trajectory shown in Fig. 9. Plotted in blue are curves of constant Tisserand parameter: a quasi-constant of motion in the circular restricted three-body problem corresponding to a first-order approximation of the Jacobi constant C_J. In terms of the osculating orbital elements a and e (semi-major axis and eccentricity, respectively), the Tisserand parameter is given by $T = 1/a + 2\sqrt{a(1-e^2)}$. The green points represent snapshots of the trajectory's orbital state at successive intersections with the CR3BP's x-axis. The orbit clearly jumps between orbital resonances with Titan, marked by the straight red lines, scarcely deviating from a curve of constant Tisserand parameter highlighted in orange. The region of the plot labelled "No Transfer Zone" corresponds to values of the Tisserand parameter for which passage between the exterior and interior regions of the Saturn-Titan-spacecraft CR3BP is energetically disallowed.

trajectory requires a surprisingly small total ΔV: just 8 m/s. As a rough comparison, a Hohmann transfer between circular Saturnian orbits with radii 1.70 and 0.74 Saturn-Titan distances requires a total ΔV of more than 2100 m/s (but takes only 11 days to traverse).

A useful graphical represention of the low-fuel trajectory just described is shown in Fig. 10. The graph displays the evolution of the pericenter and apocenter of the trajectory in juxtaposition with curves of constant Tisserand parameter: a quasi-constant of motion in the circular restricted three-body problem corresponding to a first-order approximation of the Jacobi constant C_J. The orbit clearly jumps between orbital resonances with Titan, scarcely deviating from a curve of constant Tisserand parameter. Graphs like that of Fig. 10 are studied in detail by Campagnola & Russel[27] in the context of endgame strategies for mission design.

It is not difficult to see that the trajectory of Fig. 9 could be extended to achieve a further reduction in semimajor axis and allow for visitation of Saturn's inner moons. Indeed, the last periapsis passage of the trajectory in Fig. 9 lies relatively close to the orbital path of Rhea, Saturn's second largest moon. It is important to note, however, that reproducing a Multi-Moon Orbiter trajectory like that designed for the Jovian moon system by Ross and co-authors[24] is hindered by the natural architecture of the Saturnian moon system. Unlike the Jovian moon system, where the major moons Callisto, Ganymede, and Europa have Jupiter-Moon-spacecraft CR3BP mass parameters μ on the order of 10^{-4}, the moons of Saturn other than Titan all have mass parameters μ less than 5×10^{-6}.

As the energy kick function f in the Keplerian map (17) is multiplied by a factor of μ, it follows that the maximum feasible reduction in Keplerian energy accompanying a resonant gravity assist with one of Saturn's non-Titanian moons is drastically smaller than that accompanying a gravitational assist in the Jovian moon system.

CONCLUSIONS AND FURTHER STUDY

This report has demonstrated the manner in which invariant manifold theory from the three-body problem, together with a discrete-mechanics-based optimal control algorithm, may be applied to celestial trajectory design problems. Specifically, we have exploited invariant manifolds in the Sun-Earth-spacecraft and Earth-Moon-spacecraft three-body systems to produce a fuel-efficient trajectory from the Earth to the Moon, and have expanded upon the work of Koon and co-authors[20] by employing the DMOC algorithm to minimize this trajectory's total fuel usage. We have further applied CR3BP invariant manifold theory, together with the use of resonant gravity assists, to design a fuel-efficient Saturnian moon tour analogous to the Jovian Multi-Moon Orbiter designed by Ross and co-authors.[24]

To extend the Saturnian moon tour of Fig. 9 toward visitation of Saturn's inner moons is an obvious follow-up to this study. It would also be of interest to apply DMOC to this trajectory in an effort to reduce fuel requirements; the trajectory plotted in Fig. 9 has been generated using a technique akin to multiple shooting.

A comparison of the methods described in this paper with traditional trajectory design techniques is worth investigation. In particular, how do the patched three-body motions like those of Fig. 6 compare with trajectories generated from a patched conic approach in terms of ΔV costs and flight times? How does DMOC compare with standard trajectory optimization techniques like collocation and multiple shooting? Also, what is the connection between the resonant gravity assists utilized in this report, which have been developed for low-energy regimes in the three-body problem, and standard gravity assist maneuvers that have been developed for higher-energy regimes using patched conic approximations?

Finally, it would be beneficial to refine the trajectories presented in this report using higher-fidelity models of the relevant celestial systems. The techniques that have been showcased in the preceding sections provide a toolbox for low-fuel trajectory design at the foundational level; incorporating these maneuvers into full-fledged space mission trajectories using high-fidelity ephemerides marks the next major step toward putting these ideas into practice and realizing the ever-closer dream of fuel-efficient space travel.

ACKNOWLEDGMENTS

The authors wish to thank the Caltech Summer Undergraduate Research Fellowship program and the Aerospace Corporation for their financial support.

REFERENCES

[1] E. Piazza, "News features: the story of Saturn – Cassini-Huygens mission to Saturn & Titan," 2005.
[2] A. D. Fortes, "Exobiological implications of a possible ammonia-water ocean inside Titan," *Icarus*, Vol. 146, 2000, pp. 444–452.
[3] E. R. Stofan *et al.*, "The lakes of Titan," *Nature*, Vol. 445, 2007, pp. 61–64.
[4] W. S. Koon, M. W. Lo, J. E. Marsden, and S. D. Ross, "Dynamical Systems, the Three-Body Problem, and Space Mission Design," *International Conference on Differential Equations* (B. Fiedler, K. Gröger, and J. Sprekels, eds.), Berlin, World Scientific, 2000, pp. 1167–1181.

[5] J. E. Marsden and S. D. Ross, "New methods in celestial mechanics and mission design," *Bulletin of the American Mathematical Society*, Vol. 43, 2005, pp. 43–73.
[6] W. S. Koon, M. W. Lo, J. E. Marsden, and S. D. Ross, "The Genesis trajectory and heteroclinic connections," *AAS/AIAA Astrodynamics Specialist Conference*, Girdwood, Alaska, 1999, pp. 99–451.
[7] W. S. Koon, M. Lo, J. E. Marsden, and S. D. Ross, "Heteroclinic connections between periodic orbits and resonance transitions in celestial mechanics," *Chaos*, Vol. 10, 2000, pp. 427–469.
[8] V. G. Szebehely, *Theory of Orbits: The Restricted Problem of Three Bodies*. New York: Academic Press, 1967.
[9] G. Gómez, W. S. Koon, M. Lo, J. E. Marsden, J. Masdemont, and S. D. Ross, "Invariant manifolds, the spatial three-body problem and space mission design," *AAS/AIAA Astrodynamics Specialist Conference*, Quebec City, Canada, 2001, pp. 1–20.
[10] T. S. Parker and L. O. Chua, *Practical Numerical Algorithms for Chaotic Systems*. New York: Springer-Verlag, 1989.
[11] S. D. Ross, *Cylindrical manifolds and tube dynamics in the restricted three-body problem*. PhD thesis, California Institute of Technology, Pasadena, CA, 2004.
[12] O. Junge, J. E. Marsden, and S. Ober-Blöbaum, "Discrete mechanics and optimal control," *Proceedings of the 16th IFAC Conference on Decision and Control*, Prague, 2005, pp. 1–6.
[13] A. Lew, J. E. Marsden, M. Oritz, and M. West, "An overview of variational integrators," *Finite Element Methods: 1970's and Beyond*, 2004, pp. 98–115.
[14] H. Goldstein, C. Poole, and J. Safko, *Classical Mechanics*. San Fransisco: Addison Wesley, 2002.
[15] A. Lew, J. E. Marsden, M. Oritz, and M. West, "Variational time integrators," *International Journal for Numerical Methods in Engineering*, Vol. 60, 2004, pp. 153–212.
[16] J. E. Marsden and M. West, "Discrete mechanics and variational integrators," *Acta Numerica*, Vol. 10, 2001, pp. 357–514.
[17] J. E. Marsden and T. S. Ratiu, *Introduction to Mechanics and Symmetry : A Basic Exposition of Classical Mechanical Systems*. New York: Springer, 1999.
[18] D. P. Bertsekas, *Nonlinear Programming*. Belmont, Massachusetts: Athena Scientific, 1995.
[19] M. S. Bazaraa, H. D. Sherali, and C. M. Shetty, *Nonlinear Programming : Theory and Algorithms*. New York: Wiley, 1993.
[20] W. S. Koon, M. W. Lo, J. E. Marsden, and S. D. Ross, "Shoot the Moon," *AAS/AIAA Astrodynamics Specialist Conference*, Florida, 2000, pp. 1–8.
[21] S. Kemble, *Interplanetary Mission Analysis and Design*. Berlin: Springer, 2006.
[22] W. S. Koon, M. W. Lo, J. E. Marsden, and S. D. Ross, *Dynamical Systems, the Three-Body Problem and Space Mission Design*. Springer, 2006.
[23] E. Perozzi and A. D. Salvo, "Novel spaceways for reaching the Moon: an assessment for exploration," *Celestial Mechanics and Dynamical Astronomy*, Vol. 102, 2008, pp. 207–218.
[24] S. D. Ross, W. S. Koon, M. W. Lo, and J. E. Marsden, "Design of a Multi-Moon Orbiter," *AAS/AIAA Space Flight Mechanics Meeting*, Ponce, Puerto Rico, 2008, pp. 1–15.
[25] S. D. Ross and D. J. Scheeres, "Multiple gravity assists, capture, and escape in the restricted three-body problem," *SIAM Journal on Applied Dynamical Systems*, Vol. 6, 2007, pp. 576–596.
[26] P. Grover and S. Ross, "Designing trajectories in a planet-moon environment using the controlled Keplerian map," *18th AAS/AIAA Space Flight Mechanics Meeting*, Galveston, Texas, 2008, pp. 1–12.
[27] S. Campagnola and R. Russell, "The endgame problem part B : The multi-body technique and the T-P Graph," *19th AAS/AIAA Space Flight Mechanics Meeting*, Savannah, Georgia, 2009, pp. AAS 09–227.